The parallel-sequential field subtraction techniques for nonlinear ultrasonic imaging

Cite as: AIP Conference Proceedings **1949**, 070001 (2018); https://doi.org/10.1063/1.5031553
Published Online: 20 April 2018

Jingwei Cheng, Jack N. Potter and Bruce W. Drinkwater

The Parallel-Sequential Field Subtraction Techniques for Nonlinear Ultrasonic Imaging

Jingwei Cheng[1, a)], Jack N Potter[1] and Bruce W Drinkwater[1]

[1]Department of Mechanical Engineering, University of Bristol, Queen's Building, University Walk, Bristol BS8 1TR, United Kingdom

[a)]Corresponding author: jingwei.cheng@bristol.ac.uk

Abstract. Nonlinear imaging techniques have recently emerged which have the potential to detect cracks at a much earlier stage and have sensitivity to particularly closed defects. This study utilizes two modes of focusing: *parallel*, in which the elements are fired together with a delay law, and *sequential*, in which elements are fired independently. In the parallel focusing, a high intensity ultrasonic beam is formed in the specimen at the focal point. However, in sequential focusing only low intensity signals from individual elements enter the sample and the full matrix of transmit-receive signals is recorded; with elastic assumptions, both parallel and sequential images are expected to be identical. Here we measure the difference between these images formed from the coherent component of the field and use this to characterize nonlinearity of closed fatigue cracks. In particular we monitor the reduction in amplitude at the fundamental frequency at each focal point and use this metric to form images of the spatial distribution of nonlinearity. The results suggest the subtracted image can suppress linear features (e.g., back wall or large scatters) and allow damage to be detected at an early stage.

INTRODUCTION

Nonlinear methods are sensitive to the microstructural material changes which precede macroscopic crack growth [1, 2]. Only a few of them have demonstrated the capability to spatially isolate fatigue cracks and effectively monitor their early growth [3-7]. The use of complicated bespoke setups leads to impracticality, which is one reason why these techniques have yet to see significant application by industry [8-14]. Recently, some nonlinear imaging techniques using ultrasonic phased arrays have emerged with the ability to localise and size the closed cracks [15-18]. Some of the most promising results were from nonlinear diffuse energy imaging, which demonstrated its ability to effectively isolate the location of nonlinear defects. However, when the test structures become large in size and are made of highly attenuated materials, a measurable diffuse field cannot be produced so that the data acquisition is not realizable. Other methods are restricted to poor selectivity of local nonlinearities from defects (i.e., hard to distinguish nonlinear features from background linear features).

In the present paper, the proposed technique uses the phase array to create a spatial map of nonlinearity by focusing in two modes of operation, *parallel* and *sequential*. The parallel is to fire all the elements with a pre-set delay law to physically result in high intensity focus at the target pixel, whereas the sequential is achieved by post-processing the data from full matrix capture and synthetically focusing at the pixel location. The two resulting fields would be linearly equivalent and therefore any differences can be used as measure of nonlinearity. The proposed imaging metric here is the difference in coherently scattered amplitude for fields yielded from sequential and parallel focusing at each pixel location. We demonstrate that this method can be used to detect fatigue crack growth from 15% of its fatigue life in a mild steel specimen. In addition, coherent field imaging can shorten the time for data acquisition, which potentially allows the faster imaging of particularly large structures.

44th Annual Review of Progress in Quantitative Nondestructive Evaluation, Volume 37
AIP Conf. Proc. 1949, 070001-1–070001-7; https://doi.org/10.1063/1.5031553
Published by AIP Publishing. 978-0-7354-1644-4/$30.00

METHOD

Coherent Sequential-Parallel Relative Field Imaging Nonlinear Technique (C-SPRINT)

The alternative modes of firing are realized with a standard commercially available array controller (Peak NDT Micropulse). In parallel mode, the selected transmitter elements are fired in a pre-set sequence termed a delay law. The application of this mode results in a high intensity beam forming in the test structure which can be physically translated, steered or focused. Alternatively, in sequential mode each transmitter is fired independently and the time-domain signals from all the individual combinations of transmitter-receiver pairs are captured one after the other. This so-called full matrix capture (FMC) can then be post-processed with the same delay law used in parallel transmission. Given that the test specimen is time invariant and the principle of linear superposition holds, these two modes of operation form linearly equivalent images. However, these two modes of focusing are not nonlinearly identical at the focal point due to local material nonlinearities. This physical difference allows the imaging of material nonlinearity. It should be noted that transmission energy from each transmitter is also the same for both fields, so that the bulk material, contact-acoustic and instrumentation nonlinearities generated away from focal point are equivalent between two modes.

Elastic nonlinearity may be inferred if the relative field distortion at the focal point can be measured. Assume $f_{n,m}(t)$ are the time-domain received signals for each combination of transmit (n) and receive (m) elements in the sequential case; $\delta_n(r)$ and $\delta_m(r)$ are the transmission delay and the reception delay respectively applied to the n^{th} element to achieve a focus at a point; and $g_m(r,t)$ is the time-domain signal received on element m for the parallel transmission of all elements delayed independently by $\delta_n(r)$. The frequency (ω) domain versions of $f_{n,m}(t)$ and $g_m(r,t)$ are given by $F_{n,m}(\omega) = \int_{-\infty}^{+\infty} f_{n,m}(t) e^{-i\omega t} dt$ and $G_m(\omega) = \int_{-\infty}^{+\infty} g_m(t)\, e^{-i\omega t} dt$, respectively.

In application to the kind of defect considered here, the dominant effect of the nonlinear response is a transfer of energy from fundamental band to subharmonics and superharmonics. The energy of the fundamental bandwidth is then found from integration of the) energy in the frequency domain. In this study the bandwidth from $\frac{5}{6}\omega_0$ to $\frac{7}{6}\omega_0$ was examined. In addition, the other nonlinear response, phase change of fundamental waves, can be explored and characterized due to the nonlinear defect at the focal point. Consequently, the received amplitude in the sequential focusing case A_s at focal point r for a *64* element array is given as:

$$A_s(t) = \frac{1}{\pi} \int_{\frac{5}{6}\omega_0}^{\frac{7}{6}\omega_0} \left(\sum_{m=1}^{64} \left(\sum_{n=1}^{64} F_{n,m}(\omega) e^{i\omega\delta_n(r)} \right) e^{i\omega\delta_m(r)} \right) e^{-i\omega t} d\omega \,. \tag{1}$$

Likewise, the amplitude A_p in the parallel focusing case is calculated as follows:

$$A_p(t) = \frac{1}{\pi} \int_{\frac{5}{6}\omega_0}^{\frac{7}{6}\omega_0} \left(\sum_{m=1}^{64} G_m(\omega)\, e^{i\omega\delta_m(r)} \right) e^{-i\omega t} d\omega \,. \tag{2}$$

Therefore, the amplitude intensity of the focal point r in the sequential case I_s is given as:

$$I_s(x,z) = A_s \left(\frac{\sqrt{(x_a - x)^2 + z^2} + \sqrt{(x_b - x)^2 + z^2}}{c} \right), \tag{3}$$

where x_a and x_b are the positions of reference elements in x-axis for the transmission and reception delay laws respectively. Similarly, the intensity of the focal point r in the parallel case I_p is given by:

$$I_p(x,z) = A_p \left(\frac{\sqrt{(x_a - x)^2 + z^2} + \sqrt{(x_b - x)^2 + z^2}}{c} \right), \tag{4}$$

Finally an image is formed by calculation of the nonlinear metric α at a given imaging/focal point $\alpha(x, z)$

$$\alpha(x,z) = \left| I_{\mathrm{s}}(x,z) - I_{\mathrm{p}}(x,z) \right| . \tag{5}$$

EXPERIMENTAL PROCEDURE

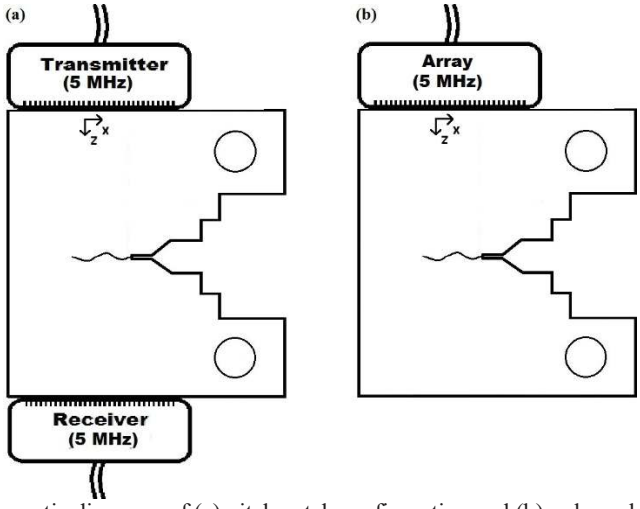

FIGURE 1. Schematic diagrams of (a) pitch-catch configuration and (b) pulse-echo configuration.

Mild steel ASTM A36 (c=5924 m s^{-1}) compact tension (CT) specimens were manufactured according to the ASTM standard E647-05. The load was varied between 2 and 15 kN in a hydraulic testing machine (Instron 8800MJ6272, UK) to ensure that the specimen failed in the high cycle fatigue regime. This fatigue test was conducted in order to monitor crack growth at early stages, hence the loading step was chosen as 10000 cycles and the test was stopped at 40000 cycles. The microstructure around the crack tip was observed by a microscope (Zeiss Axio Imager 2, Germany) and, consequently, the crack length was measured periodically during the fatigue test.

The ultrasonic measurements using C-SPRINT were implemented through positioning an array as the transmitter on the top face in Figs. 1(a) and (b). At reception, two different configurations (termed pulse echo and pitch catch) have been applied so that the backscattered and through transmitted waves were able to be captured respectively. It should be noted that although the pitch catch arrangement might not be practically realizable due to access limitations, it provides the best case scenario for capturing the fundamental signals transmitting through closed cracks since the entire field that propagates through the defect is recovered. For the pitch catch method, the other array is placed on the opposite face in Fig. 1 (a). All the measurements were performed with 64 element ultrasonic arrays (Imasonic, France) with nominal frequency of 5 MHz, and pitch of 0.63 mm, as well as an array controller (Peak NDT Micropulse FMC, UK).

EXPERIMENTAL RESULTS

The proposed technique demonstrated its capability to localize the crack tip and size the cracks at early stages. The underlying physics behind the nonlinear image was explored to understand the nonlinear responses with crack growth. Two fundamental physical quantities (absolute amplitude and phase), of which the nonlinear image consists, were studied respectively over the considered bandwidth.

Pitch-Catch Imaging

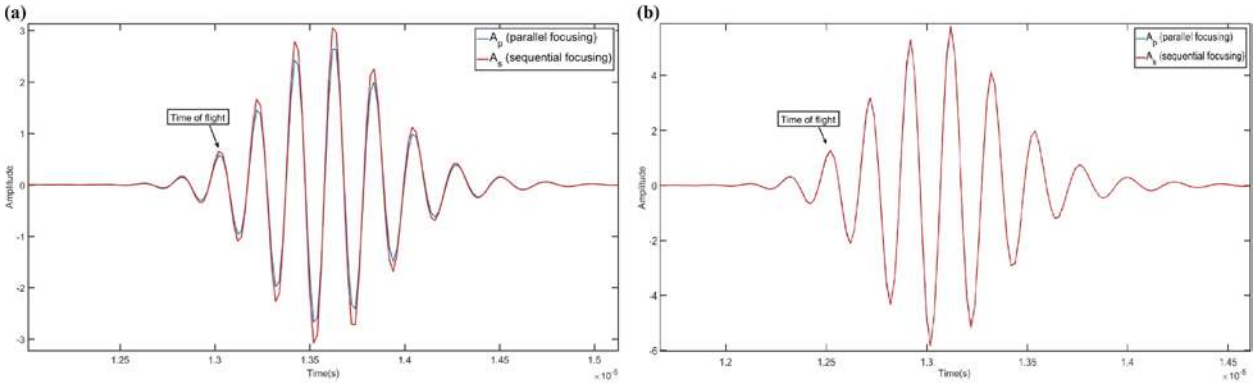

FIGURE 2. Time traces at 30000 loading cycles, (a) focusing at crack tip, and at (b) undamaged point.

The pitch catch configuration is expected to be the most sensitive to crack closure. The entire wave front passing through the closed cracks is allowed to be captured by positioning another array on the opposite side. Although this configuration is often impractical for many applications, it is worth investigating the nonlinear phenomenon prior to the formation of partially linear defects.

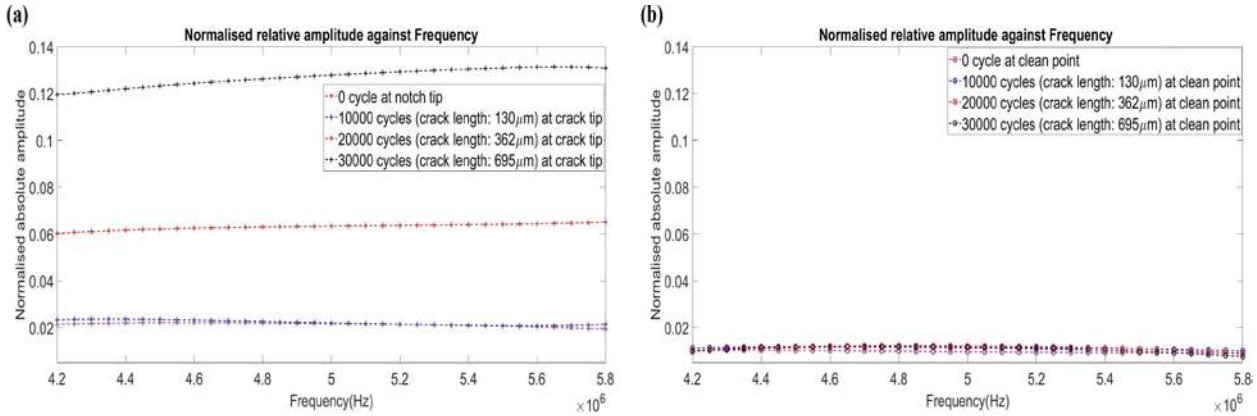

FIGURE 3. Normalized relative absolute amplitude against frequency with increasing loading cycles, (a) focusing at crack tip and (b) undamaged clean point.

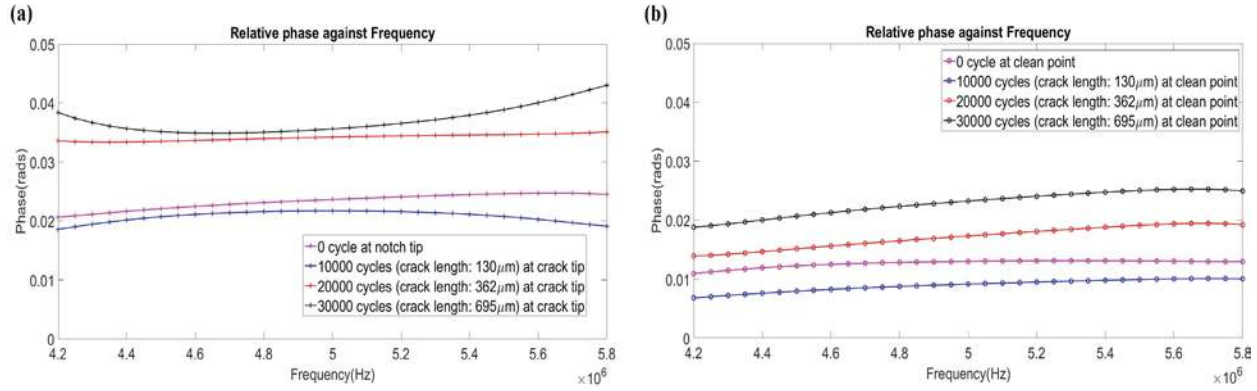

FIGURE 4. Relative phase against frequency with increasing loading cycles, (a) focusing at crack tip and (b) undamaged clean point.

As the significant change in amplitude has been observed from time traces focused at the damaged point (shown in Fig. 2(a)), the normalized relative absolute amplitude between parallel and sequential focusing is first studied and can be expressed as: $\delta_A(\omega) = \frac{|A_s(\omega)|-|A_p(\omega)|}{|A_s(\omega)|}$. Note that 5 cycle windowed signals centered at focal time were post-processed for this frequency analysis. The normalized amplitude is used to evaluate the difference in absolute amplitude between the two different focusing methods with crack growth. Figure 3(a) shows that the relative amplitude parameter when focused at the tip increases significantly with increasing crack length from 0 cycle to 30000 cycles. For comparison, as shown in Fig. 3(b), a fixed clean point, considered as undamaged area, was chosen to understand the background level. Results suggest that all of their relative amplitude remain at the low level in close proximity to the first two cycles observed in Fig. 3(a). Therefore, it is evident that the absolute amplitude allows for the characterization and localization the nonlinear defect. On the other hand, Figs. 4(a) and (b) demonstrate the relationship between the relative phase ($\delta_\varphi(\omega) = arg\big(A_s(\omega)\big) - arg\left(A_p(\omega)\right)$ and crack length over the same frequency band. Consistent results show that the relative phase increases, especially at the crack tip. Note that the increase here is not as dominant as the one in Fig. 3(a), and the small variance between all the cycles at the linear pixel might be due to inherent noise arising from coupling change, local material and instrumentation nonlinearities.

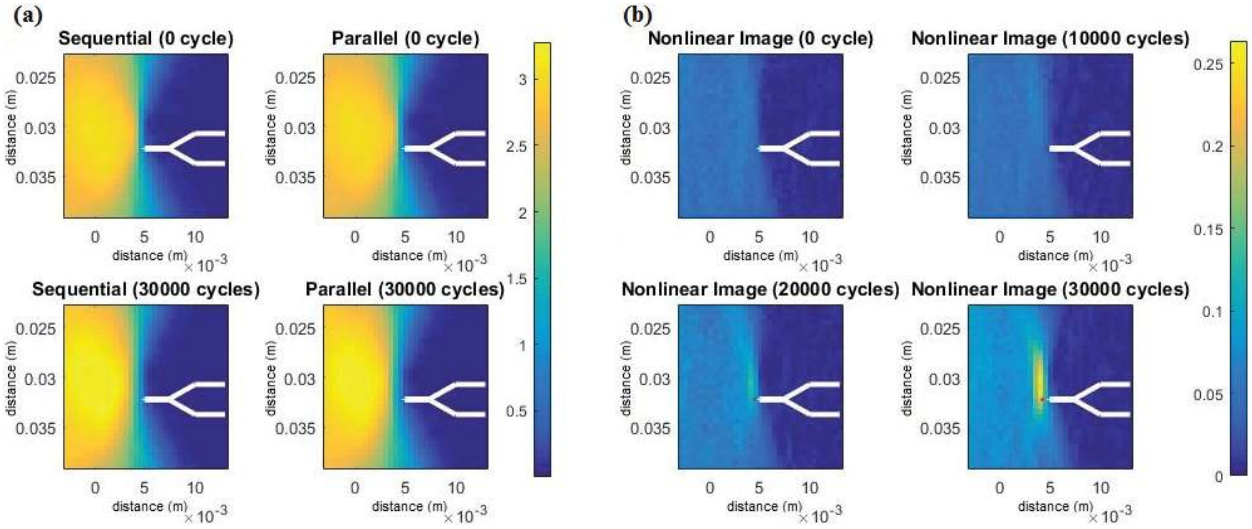

FIGURE 5. (a) Two extreme cases of linear sequential and parallel images in arbitrary units and (b) nonlinear images from 0 cycle to 30000 cycles in nonlinear metric, α.

Consequently, the nonlinear features induced from difference in both amplitude and phase can be imaged if the parallel image is subtracted from the sequential. Figure 5(a) presents two extreme cases of sequential and parallel images in which the identical background features with close magnitude are displayed. Note that linear geometries of the notch are plotted with white lines. Although their features are always indistinguishable from crack growth, the subtracted images in Fig. 5(b) demonstrate its capability of not only suppressing the geometric features, but also localizing and sizing cracks. The earliest detection was at 20000 cycles, where the maximum nonlinearities are focused at the crack tip, indicated by the red cross in Fig. 5(b). At 30000 cycles, the nonlinear response became significantly higher with more extensive cracking (observed by microscope). For such nonlinear features the image produced is that of the dominant change in amplitude, small phase offset and associated point spread function for the technique.

Pulse-Echo Imaging

Results from the pitch catch arrangement presented high selectivity of closed cracks from 20000 cycles. However, only one-side access is often available in many practical operations. The feasibility of pulse-echo configuration is, therefore, investigated in terms of change in phase and absolute amplitude. For this single-side approach, the linear backscatter in the vicinity of nonlinear defect is needed in order to capture the forward field originally distorted by closed cracks. On the other hand, the nonlinearities cannot be detected until the linear scattering features are formed (i.e., the detection is less sensitive to the early closed cracks).

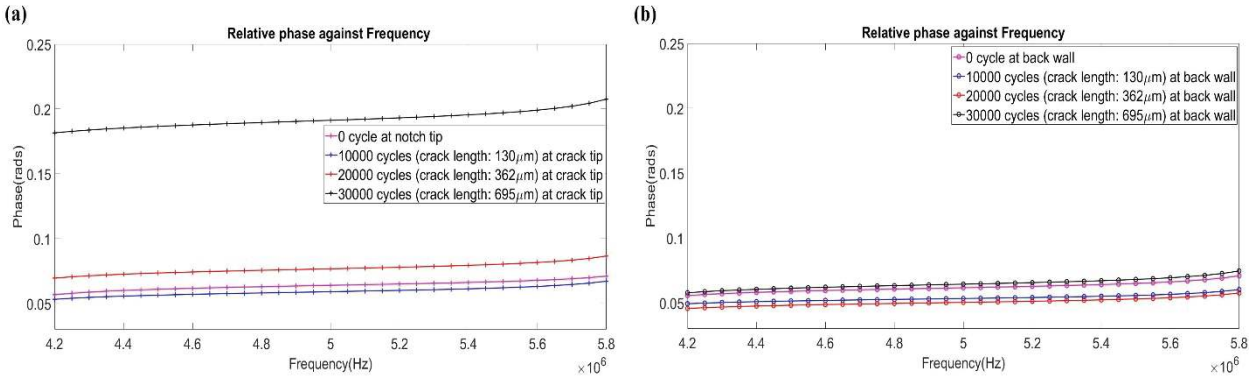

FIGURE 6. Relative phase against frequency with increasing loading cycles, (a) focusing at crack tip and (b) back wall.

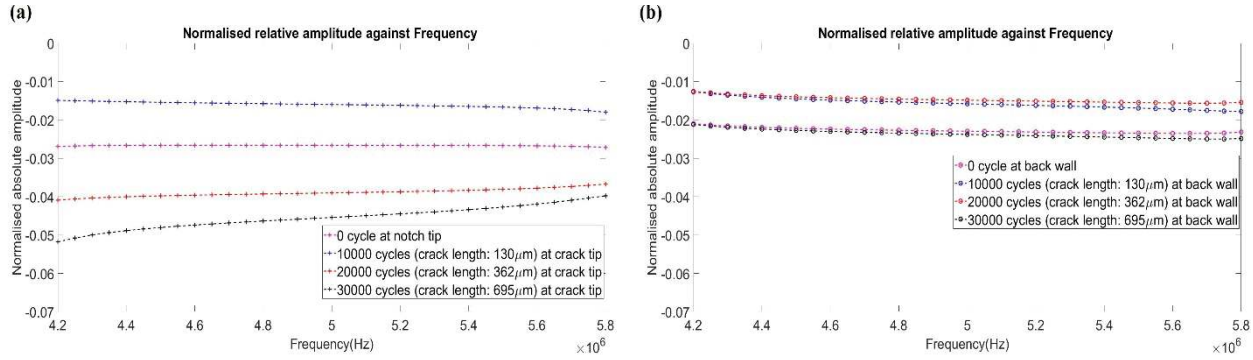

FIGURE 7. Normalized absolute amplitude against frequency with increasing loading cycles, (a) focusing at crack tip and (b) back wall.

Figures 6(a) and (b) present the study between relative phase, $\delta_{\varphi}(\omega)$ and crack length by focusing at the crack tip and the notch edge. In contrast to previous results from the pitch-catch, the relative phase is dominant in nonlinear responses. As shown in Fig. 6(a), there was a significant increase between 20000 and 30000 cycles. Despite the fact that some correlation between relative amplitude, $\delta_{A}(\omega)$ and crack length was observed in Fig. 7(a), systematic errors limit the repeatability of measurements and possibly produce those small variances.

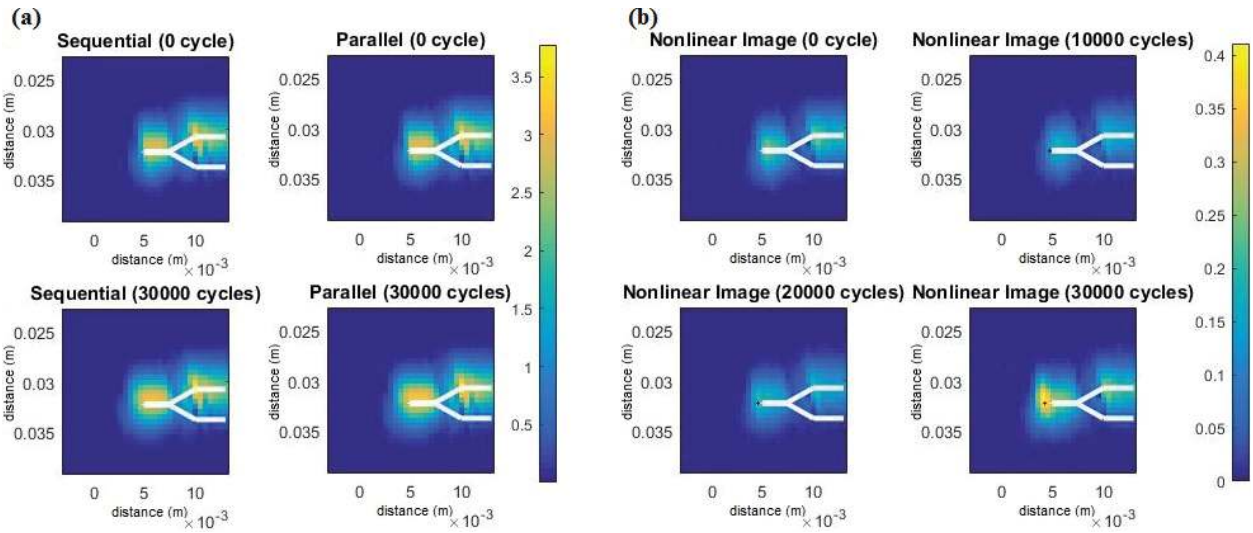

FIGURE 8. (a) Two extreme cases of linear sequential and parallel images in arbitrary units and (b) nonlinear images from 0 cycle to 30000 cycles in nonlinear metric, α.

The linear geometric features are presented with parallel and sequential imaging in Fig. 8(a), and the linear and nonlinear features cannot be distinguished with crack growth. Likewise, the nonlinear features can be imaged if the parallel data is subtracted from the sequential. As shown in Fig. 8(b), the crack tip was precisely localized at 30000 cycles and results here are consistent to those from pitch-catch configuration. Moreover, some residual linear background features (presented in Fig. 8(b)) possibly arise from inherent system errors between two modes of operation and local material nonlinearities.

CONCLUSIONS

The C-SPRINT method is proposed to effectively monitor fatigue crack growth and demonstrated in mild steel from 400 μm (circa. 15% of fatigue life). Localization of crack tip is realizable from observing the peak nonlinear metric. In addition, effective suppression of linear features has been demonstrated, providing the ability to distinguish the nonlinear defect from other geometric features. We note that those residual background features can be potentially improved if the inherent noise in phase and amplitude is compensated. Regardless, this technique enhances sensitivity and selectivity, as well as reduces the time for data acquisition.

REFERENCES

1. P. B. Nagy, Fatigue damage assessment by nonlinear ultrasonic materials characterization, *Ultrasonics* **36**, 375-381 (1998).
2. K. H. Matlack, J-Y Kim, L. J. Jacobs and J. Qu, Review of second harmonic generation measurement techniques for material state determination in metals, *J. Nondestruct. Eval*. **34**, 273 (2015).
3. Z. Su, C. Zhou, M. Hong, L. Cheng, Q. Wang and X. Qing, Acousto-ultrasonics-based fatigue damage characterization: linear versus nonlinear signal features, *Mech. Syst. Signal Process* **45**, 225-239 (2014).
4. H. J. Lim, B. Song, B. Park and H. Sohn, Noncontact fatigue crack visualization using nonlinear ultrasonic modulation, *NDT&E Int* **73**, 8-14 (2015).
5. G. P. M. Fierro and M. Meo, Residual fatigue life estimation using a nonlinear ultrasound modulation method, *Smart Mater. Struct*. **24**, 025040 (2015).
6. H. J. Lim and H. Sohn, Fatigue crack detection using structural nonlinearity reflected on linear ultrasonic features, *J. Appl. Phys*. **118**, 244902 (2015).
7. M. Amura, M. Meo and F. Amerini, Baseline-free estimation of residual fatigue life using a third order acoustic nonlinear parameter, *J. Acoust. Soc. Am.* **130**, 1829-1837 (2011).
8. J-Y Kim, L. J. Jacobs, J. Qu and J. W. Littles, Experimental characterization of fatigue damage in a nickel-base superalloy using nonlinear ultrasonic wave, *J. Acoust. Soc. Am*. **120**, 1266-1273 (2006).
9. J. H. Cantrell and W. T. Yost, Nonlinear ultrasonic characterization of fatigue microstructures, *Int. J. Fatigue* **23**, 487-490 (2001).
10. I. Solodov, J. Wackerl, K. Pfleiderer and G. Busse, Nonlinear self-modulation and subharmonic acoustic spectroscopy for damage detection and location, *Appl. Phys. Lett*. **84**, 5386-5388 (2004).
11. A. J. Croxford, P. D. Wilcox and B. W. Drinkwater and P. B. Nagy, The use of non-collinear mixing for nonlinear ultrasonic detection of plasticity and fatigue, *J. Acoust. Soc. Am*. **126**, 117-122 (2009).
12. Y. Ohara, S. Horinouchi, M. Hashimoto, Y. Shintaku and K. Yamanaka, Nonlinear ultrasonic imaging method for closed cracks using subtraction of responses at different external loads, *Ultrasonics* **51**, 661-666 (2010).
13. Z. YAN and P. B. Nagy, Thermo-optical modulation for improved ultrasonic fatigue crack detection in Ti-6Al-4V, *NDT&E Int.* **33**, 213-223 (2000).
14. J.P. Jiao, B. W. Drinkwater, S. A. Neild and P. D. Wilcox, Low-frequency vibration modulation of guided waves to image nonlinear scatters for structural health monitoring, *Smart Mater. Struct*. **18**, 065006 (2009).
15. J. N. Potter, A. J. Croxford and P. D. Wilcox, Nonlinear ultrasonic phased array imaging, *Phys. Rev. Lett*. **113**, 144301 (2014).
16. J. Cheng, J. N. Potter, A. J. Croxford and B. W. Drinkwater, Monitoring fatigue crack growth using nonlinear ultrasonic phased array imaging, *Smart Mater. Strct*. **26**, 055006 (2017).
17. Y. Ohara, T. Mihara, R. Sasaki, T. Ogata, S. Yamamoto, Y. Kishimoto and K. Yamanaka, Imaging of closed cracks using nonlinear response of elastic waves at subharmonic frequency, *Appl. Phys. Lett*. **90**, 011902 (2007).
18. S. Haupert, G. Renaud and A. Schumm, Ultrasonic imaging of nonlinear scatters buried in a medium, *NDT&E Int*. **87**, 1-6 (2017).